PERFORMANCE ANALYSIS OF DFIG AS WIND ENERGY CONVERSION SYSTEMS AND SHUNT ACTIVE FILTER

A. Rajendar[1], S. Gopal Reddy[2]

[1] *Student, EEE Department, Jyothismathi Institute of technology & Science, Telangana, India*
[2] *Assoc.Prof, EEE Department, Jyothismathi Institute of technology & Science, Telangana, India*

ABSTRACT

This paper presents the operation of doubly fed induction generator (DFIG) with an integrated active filter capabilities using grid-side converter (GSC). The main contribution of this work lies in the control of GSC for supplying harmonics in addition to its slip power transfer. The rotor-side converter (RSC) is used for attaining maximum power extraction and to supply required reactive power to DFIG. This wind energy conversion system (WECS) works as a static compensator (STATCOM) for supplying harmonics even when the wind turbine is in shutdown condition. Control algorithms of both GSC and RSC are presented in detail. The proposed DFIG-based WECS is simulated using MATLAB/Simulink. A simulation of the proposed DFIG based WECS is developed using MATLAB/SIMULINK software. Simulated results are validated with test results of the developed DFIG for different practical conditions, such as variable wind speed and unbalanced/single phase loads.

Keyword: - *DFIG, STATCOM, DISTRIBUTION GENERATION*

1. INTRODUCTION

The energy demand has increased significantly. However, the conventional energy sources such as coal, oil, and gas are limited in nature. Now, there is a need for renewable energy sources for the future energy demand [1]. The other main advantages of this renewable source are eco-friendliness and unlimited in nature [2]. Due to technical advancements, the cost of the wind power produced is comparable to that of conventional power plants. Therefore, the wind energy is the most preferred out of all renewable energy sources [3]. In the initial days, wind turbines have been used as fixed speed wind turbines with squirrel cage induction generator and capacitor banks. Most of the wind turbines are fixed speed because of their simplicity and low cost [4]. By observing wind turbine characteristics, one can clearly identify that for extracting maximum power, the machine should run at varying rotor speeds at different wind speeds. Using modern power electronic converters, the machine is able to run at adjustable speeds [5]. Therefore, these variable speed wind turbines are able to improve the wind energy production [6]. Out of all variable speed wind turbines, doubly fed induction generators (DFIGs) are preferred because of their low cost [7]. The other advantages of this DFIG are the higher energy output, lower converter rating, and better utilization of generators [8]. These DFIGs also provide good damping performance for the weak grid [9]. Independent control of active and reactive power is achieved by the decoupled vector control algorithm presented in [10] and [11]. This vector control of such system is usually realized in synchronously rotating reference frame oriented in either voltage axis or flux axis. In this work, the control of rotor-side converter (RSC) is implemented in voltage-oriented reference frame.

Grid code requirements for the grid connection and operation of wind farms are discussed in [12]. Response of DFIG-based wind energy conversion system (WECS) to grid disturbance is compared to the fixed speed WECS in [13]. As the wind penetration in the grid becomes significant, the use of variable speed WECS for supplementary jobs such as power smoothening and harmonic mitigation are compulsory in addition to its power generation. This power smoothening is achieved by including super magnetic energy storage systems as proposed in [14]. The other auxiliary services such as reactive power requirement and transient stability limit are achieved by including static compensator (STATCOM) in [15]. A distribution STATCOM (DSTATCOM) coupled with fly-wheel energy storage system is used at the wind farm for mitigating harmonics and frequency disturbances [16]. However, the authors have used two more extra converters for this purpose.

A super capacitor energy storage system at the dc link of unified power quality conditioner (UPQC) is proposed in [17] for improving power quality and reliability. In all above methods, the authors have used separate converters for compensating the harmonics and also for controlling the reactive power. However, in later stages, some of the researchers have modified the control algorithms of already existed DFIG converters for mitigating the power quality problems and reactive power compensation. The harmonics compensation and reactive power control are achieved with the help of existing RSC.

Therefore, harmonics are injected from the RSC into the rotor windings. This creates losses and noise in the machine. These different harmonics in rotating part may also create mechanical unbalance. Moreover, both reactive power compensation and harmonic compensation are achieved in all these methods using RSC control. These methods increase the RSC rating. Harmonic compensation and reactive power control are done using GSC. Therefore, the harmonics are not passing through machine windings in all these cases. Todeschini and Emanuel have compared three different control algorithms and finally concluded that combined modulation of both RSC and GSC are needed for compensating the harmonics and controlling the reactive power. However, the authors have used direct current control of GSC. Therefore, harmonic compensation is not so effective and total harmonic distortion (THD) is not less than 5% as per IEEE-519 standard given in Table I. The authors have also not verified simulation results experimentally. An indirect current control technique is simple and shows better performance for eliminating harmonics as compared to direct current control.

2. PROPOSED TECHNIQUE

Fig. 1 shows a schematic diagram of the proposed DFIG based WECS with integrated active filter capabilities. In DFIG, the stator is directly connected to the grid as shown in Fig. 1. Two back-to-back connected voltage source converters (VSCs) are placed between the rotor and the grid. Nonlinear loads are connected at PCC as shown in Fig. 1. The proposed DFIG works as an active filter in addition to the active power generation similar to normal DFIG. Harmonics generated by the nonlinear load connected at the PCC distort the PCC voltage. These nonlinear load harmonic currents are mitigated by GSC control, so that the stator and grid currents are harmonic-free. RSC is controlled for achieving maximum power point tracking (MPPT) and also for making unity power factor at the stator side using voltage-oriented reference frame. Synchronous reference frame (SRF) control method is used for extracting the fundamental component of load currents for the GSC control.

2.1 DESIGN OF DFIG-BASED WECS

Selection of ratings of VSCs and dc-link voltage is very much important for the successful operation of WECS. The ratings of DFIG and dc machine used in this experimental system are given in Appendix. In this section, a detailed design of VSCs and dc-link voltage is discussed for the experimental system used in the laboratory.

2.2.1 Selection of DC-Link Voltage

Normally, the dc-link voltage of VSC must be greater than twice the peak of maximum phase voltage. The selection of dc-link voltage depends on both rotor voltage and PCC voltage. While considering from the rotor side, the rotor voltage is slip times the stator voltage. DFIG used in this prototype has stator to rotor turns ratio as 2:1. Normally, the DFIG operating slip is ±0.3. So, the rotor voltage is always less than the PCC voltage. So, the design criteria for the selection of dc-link voltage can be achieved by considering only PCC voltage. While considering from the GSC side, the PCC line voltage (*vab*) is 230 V, as the machine is connected in delta mode.

$$V_{\mathrm{dc}} \geq \frac{2\sqrt{2}}{\sqrt{3} * m} V_{ab} \qquad (1)$$

Therefore, the dc-link voltage is estimated as

where *Vab* is the line voltage at the PCC. Maximum modulation index is selected as 1 for linear range. The value of dc-link voltage (*V*dc) by (1) is estimated as 375 V. Hence, it is selected as 375 V.

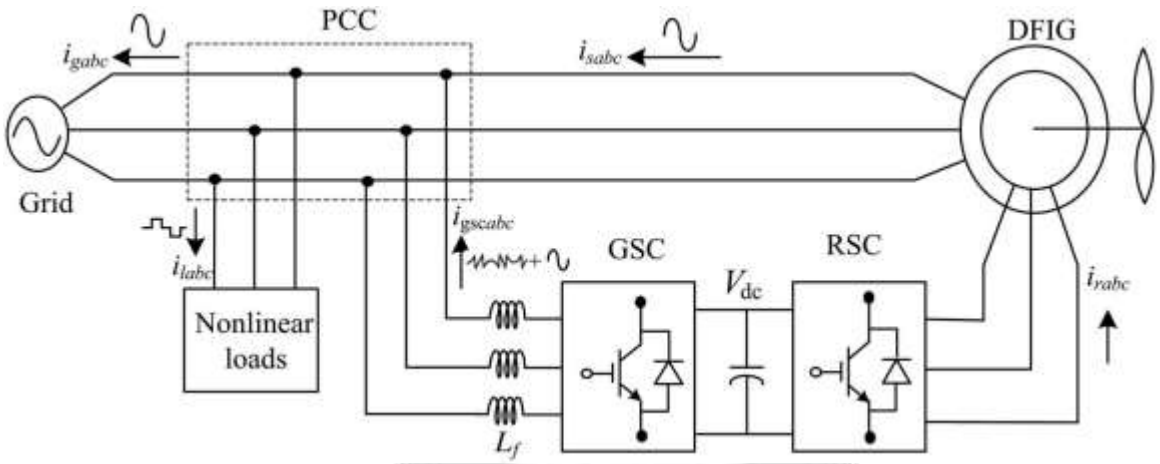

Fig-1: Proposed system configuration.

2.2.2 Selection of VSC Rating

The DFIG draws a lagging volt-ampere reactive (VAR) for its excitation to build the rated air gap voltage. It is calculated from the machine parameters that the lagging VAR of 2 kVAR is needed when it is running as a motor. In DFIG case, the operating speed range is 0.7 to 1.3 p.u. Therefore, the maximum slip (*s*max) is 0.3. For making unity power factor at the stator side, reactive power of 600 VAR (*S*max ∗ *Q*s= 0.3 ∗ 2 kVAR) is needed from the rotor side (*Q*rmax). The maximum rotor active power is (*S*max ∗ *P*). The power rating of the DFIG is 5 kW. Therefore, the maximum rotor active power (*P*rmax) is 1.5 kW (0.3 ∗ 5 kW = 1.5 kW). So, the rating of the VSC used as RSC S_{rated} is given as

$$S_{\text{rated}} = \sqrt{P_{r\max}^2 + Q_{r\max}^2}. \quad (2)$$

Thus, kVA rating of RSC *S*rated is calculated as 1.615 kVA

2.2.3 Design of Interfacing Inductor

The design of interfacing inductors between GSC and PCC depends upon allowable GSC current limit (*i*gscpp), dc-link voltage, and switching frequency of GSC. Maximum possible GSC line currents are used for the calculation. Maximum line current depends upon the maximum power and the line voltage at GSC. The maximum possible power in the GSC is the slip power. In this case, the slip power is 1.5 kW. Line voltage (*VL*) at the GSC is 230 V (the machine is connected in delta mode). So, the line current is obtained as *I*gsc = 1.5 kW/(√3 ∗ 230) = 3.765 A. Considering the peak ripple current as 25% of rated GSC current, the inductor value is calculated as

$$L_i = \frac{\sqrt{3}\, \text{mv}_{dc}}{12 a f_m \Delta i_{gsc}}$$

$$= \frac{\sqrt{3} \times 1 \times 375}{12 \times 1.5 \times 10\,000 \times 0.25 \times 3.76} = 3.8 \text{ mH}. \quad (3)$$

Interfacing inductor between PCC and GSC is selected as 4 mH.

3 CONTROL STRATEGIES

Control algorithms for both GSC and RSC are presented in this section. Complete control schematic is given in Fig. 2. The control algorithm for emulating wind turbine characteristics using dc machine and Type A chopper is also shown in Fig. 2.

3.1 Control of RSC

The main purpose of RSC is to extract maximum power with independent control of active and reactive powers. Here, the RSC is controlled in voltage-oriented reference frame. Therefore, the active and reactive powers are controlled by controlling direct and quadrature axis rotor currents (*i*dr and *i*qr), respectively. Direct axis reference rotor current is selected such that maximum power is extracted for a particular wind speed. This can be achieved by running the DFIG at a rotor speed for a particular wind speed. Therefore, the outer loop is selected as a speed controller for achieving direct axis reference rotor current (*i* ∗dr) as

$$i_{\mathrm{dr}}^{*}(k)=i_{\mathrm{dr}}^{*}(k-1)+k_{\mathrm{pd}}\left\{\omega_{\mathrm{er}}(k)-\omega_{\mathrm{er}}(k-1)\right\}+k_{\mathrm{id}}\omega_{\mathrm{er}}(k) \tag{4}$$

Where the speed error (ωer) is obtained by subtracting sensed speed (ωr) from the reference speed ($\omega * r$). $k$pd and $k$id are the proportional and integral constants of the speed controller. ωer(k) and ωer($k-1$) are the speed errors at kth and ($k-1$)th instants. i*dr(k) and i*dr($k-1$) are the direct axis rotor reference current at kth and ($k-1$)th instants. Reference rotor speed ($\omega * r$) is estimated by optimal tip speed ratio control for a particular wind speed.

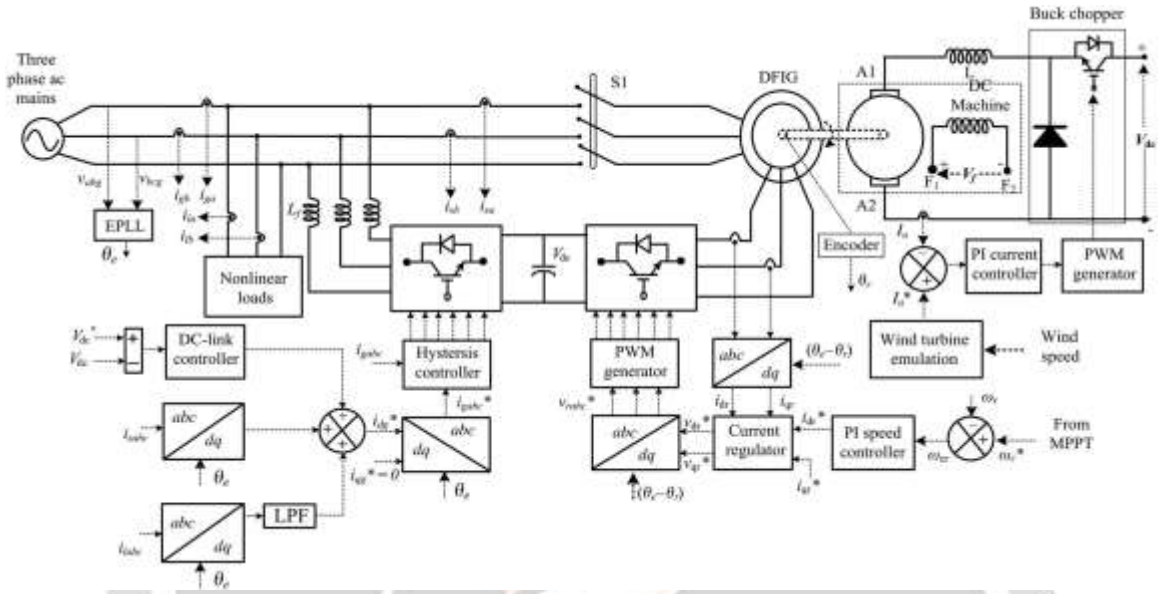

Fig-2: Control algorithm of the proposed WECS.

The tuning of PI controllers used in both RSC and GSC are achieved using Ziegler Nichols method. Initially, $k$id value is set to zero and the value of $k$pd was increased until the response stars oscillating with a period of Ti. Now, the value of $k$pd is taken as 0.45 $k$pd and $k$id is taken as 1.2 $k$pd/Ti.

Normally, the quadrature axis reference rotor current ($i*$qr) is selected such that the stator reactive power (Qs) is made zero. In this DFIG, quadrature axis reference rotor current ($i*$qr) is selected for injecting the required reactive power. Inner current control loops are taken for control of actual direct and quadrature axis rotor currents ($i$dr and $i$qr) close to the direct and quadrature axis reference rotor currents ($i*$dr and $i*$qr). The rotor currents $i$dr and $i$qr are calculated from the sensed rotor currents (ira, irb, and irc) as [32]

$$\mathrm{i_{dr}}=2/3\begin{bmatrix} i_{ra}\sin\theta_{\mathrm{slip}}+i_{rb}\sin(\theta_{\mathrm{slip}}-2\pi/3) \\ +i_{rc}\sin(\theta_{\mathrm{slip}}+2\pi/3)\end{bmatrix} \tag{5}$$

$$\mathrm{i_{qr}}=2/3\begin{bmatrix} i_{ra}\cos\theta_{\mathrm{slip}}+i_{rb}\cos(\theta_{\mathrm{slip}}-2\pi/3) \\ +i_{rc}\cos(\theta_{\mathrm{slip}}+2\pi/3)\end{bmatrix} \tag{6}$$

where slip angle (θslip) is calculated as

$$\theta_{\mathrm{slip}}=\theta_e-\theta_r \tag{7}$$

where θe is calculated from PLL for aligning rotor currents into voltage axis. The rotor position (θr) is achieved with an encoder. Direct and quadrature axis rotor voltages (v_dr and v_qr) are obtained from direct and quadrature axis rotor current errors ($i$der and $i$qer) as

$$v'_{\mathrm{dr}}(k) = v'_{\mathrm{dr}}(k-1) + k_{\mathrm{pdv}}\{i_{\mathrm{der}}(k) - i_{\mathrm{der}}(k-1)\} + k_{\mathrm{idv}} i_{\mathrm{der}}(k) \quad (8)$$

$$v'_{\mathrm{qr}}(k) = v'_{\mathrm{qr}}(k-1) + k_{\mathrm{pqv}}\{i_{\mathrm{qer}}(k) - i_{\mathrm{qer}}(k-1)\} + k_{\mathrm{iqv}} i_{\mathrm{qer}}(k) \quad (9)$$

$$i_{\mathrm{der}} = i^*_{\mathrm{dr}} - i_{\mathrm{dr}} \text{ and } i_{\mathrm{qer}} = i^*_{\mathrm{qr}} - i_{\mathrm{qr}} \quad (10)$$

where *k*pdv and *k*idv are the proportional and integral gains of direct axis current controller. *k*pqv and *k*iqv are the proportional and integral gains of quadrature axis current controller. Direct and quadrature components are decoupled by adding some compensating terms as [26]

$$v^*_{\mathrm{dr}} = v'_{\mathrm{dr}} + (\omega_e - \omega_r)\sigma L_r i_{\mathrm{qr}} \quad (11)$$

$$v^*_{\mathrm{qr}} = v'_{\mathrm{qr}} - (\omega_e - \omega_r)(L_m i_{ms} + \sigma L_r i_{\mathrm{dr}}). \quad (12)$$

These reference direct and quadrature voltages (*v*∗dr, *v*∗qr) are converted into three phase reference rotor voltages (*v*∗*ra*, *v*∗*rb*, *v*∗*rc*) as [32]

$$v^*_{ra} = v^*_{\mathrm{dr}} \sin\theta_{\mathrm{slip}} + v^*_{\mathrm{qr}} \cos\theta_{\mathrm{slip}} \quad (13)$$

$$v^*_{rb} = v^*_{\mathrm{dr}} \sin(\theta_{\mathrm{slip}} - 2\pi/3) + v^*_{\mathrm{qr}} \cos(\theta_{\mathrm{slip}} - 2\pi/3) \quad (14)$$

$$\mathrm{v}^*_{rc} = \mathrm{v}^*_{\mathrm{dr}} \sin(\theta_{\mathrm{slip}} + 2\pi/3) + \mathrm{v}^*_{\mathrm{qr}} \cos(\theta_{\mathrm{slip}} + 2\pi/3). \quad (15)$$

These three phase rotor reference voltages (*v*∗*ra*, *v*∗*rb*, *v*∗*rc*) are compared with triangular carrier wave of fixed switching frequency for generating pulse-width modulation (PWM) signals for the RSC.

B. Control of GSC

The novelty of this work lies in the control of this GSC for mitigating the harmonics produced by the nonlinear loads. The control block diagram of GSC is shown in Fig. 2. Here, an indirect current control is applied on the grid currents for making them sinusoidal and balanced. Therefore, this GSC supplies the harmonics for making grid currents sinusoidal and balanced. These grid currents are calculated by subtracting the load currents from the summation of stator currents and GSC currents. Active power component of GSC current is obtained by processing the dc-link voltage error (*v*dce) between reference and estimated dc-link voltage (*V* _dc and *V*dc) through PI controller as

$$i^*_{\mathrm{gsc}}(k) = i^*_{\mathrm{gsc}}(k-1) + k_{\mathrm{pdc}}\{v_{\mathrm{dce}}(k) - v_{\mathrm{dce}}(k-1)\} + k_{\mathrm{idc}} v_{\mathrm{dce}}(k) \quad (16)$$

where *k*pdc and *k*idc are proportional and integral gains of dc-link voltage controller. *V*dce(*k*) and *V*dce(*k* − 1) are dc-link voltage errors at *k*th and (*k*−1)th instants. *i*∗gsc(*k*) and *i*gsc(*k* − 1) are active power component of GSC current at *k*th and (*k*−1)th instants. Active power component of stator current (*ids*) is obtained from the sensed stator currents (*isa*, *isb*, and *isc*) using *abc* to *dq* transformation as [32]

$$i_{ds} = 2/3\,[i_{sa}\sin\theta_e + i_{sb}\sin(\theta_e - 2\pi/3) + i_{sc}\sin(\theta_e + 2\pi/3)]. \quad (17)$$

Fundamental active load current (*ild*) is obtained using SRF theory [33]. Instantaneous load currents (*ilabc*) and the value of phase angle from EPLL are used for converting the load currents in to synchronously rotating *dq* frame

(*_ild*). In synchronously rotating frames, fundamental frequency currents are converted into dc quantities and all other harmonics are converted into non-dc quantities with a frequency shift of 50 Hz. DC values of load currents in synchronously rotating *dq* frame (*ild*) are extracted using low-pass filter (LPF).

Direct axis component of reference grid current (*igd*) is obtained from the direct axis current of stator current (*ids*) and load current (*ild*) in synchronously rotating frame and the loss component of GSC current (*igsc*) as

$$\mathrm{i}_{gd}^{*} = \mathrm{i}_{gsc}^{*} + i_{ds} - \overline{i_{ld}}. \qquad (18)$$

Quadrature axis component of reference grid current (*igq*) is selected as zero for not to draw any reactive power from grid. Reference grid currents (*iga, igb*, and *igc*) are calculated from the direct and quadrature axis grid currents (*igd, i*∗*gq*) [32].

The hysteresis current controller is used to generate switching pulses for the GSC. The hysteresis controller is a feedback current control where sensed current tracks the reference current within a hysteresis band (*ihb*) [34]. At every sampling instant, the actual current (*igabc*) is compared to the reference current (*igabc*) as

$$\Delta i_{gabc} = i_{gabc}^{*} - i_{gabc} \qquad (19)$$

$$\text{when } \Delta i_{gabc} > i_{\mathrm{hb}}, \text{ lower switch is turned ON} \qquad (20)$$

$$\text{when } \Delta i_{gabc} < -i_{\mathrm{hb}}, \text{ upper switch is turned ON.} \qquad (21)$$

Using these equations, gating pulses for three phases of GSC are generated in the same way

4 SIMULATION RESULTS

The simulated results are presented in this section for validating steady-state and dynamic performances of this proposed DFIG with integrated active filter capabilities. In this section, the working of this proposed GSC is presented as an active filter even when the wind turbine is in shutdown condition. The power that is coming into the PCC through GSC is considered as positive in this thesis.

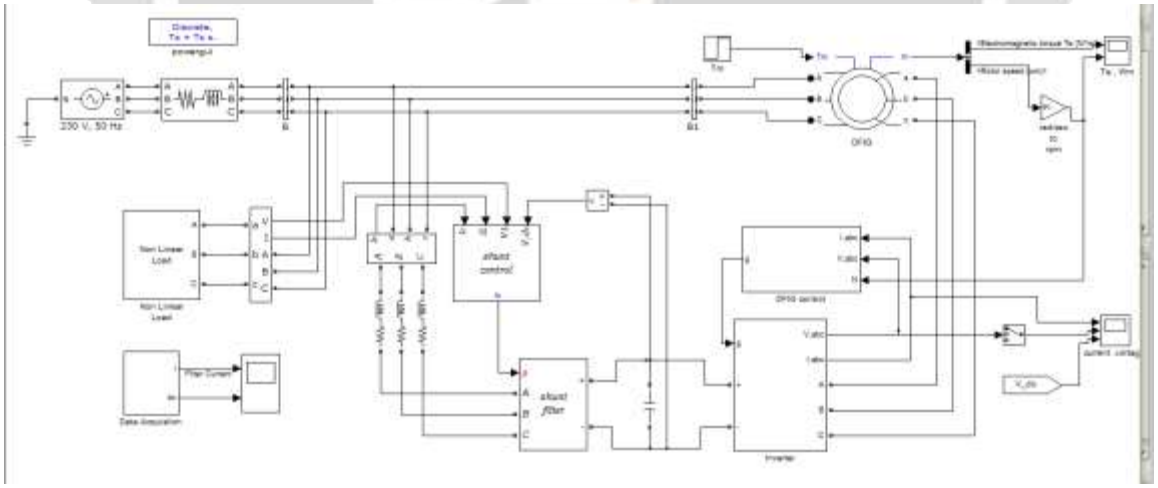

Fig-3: Proposed circuit design using MATLAB

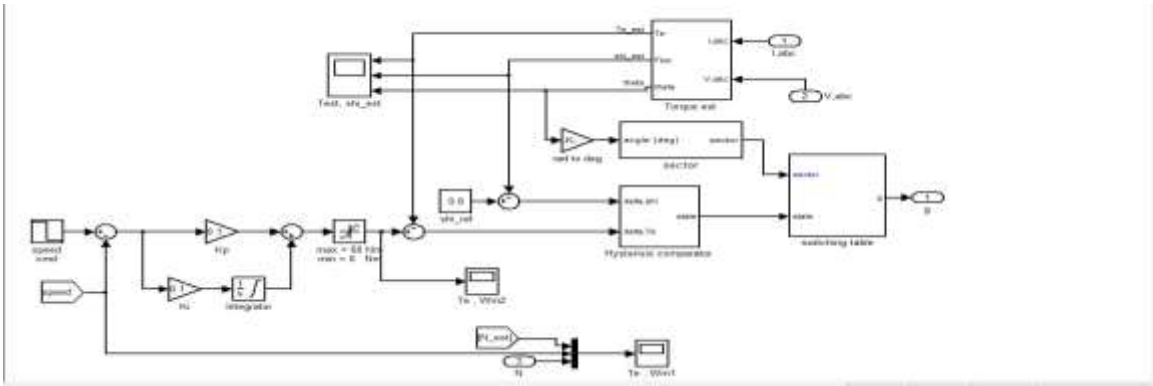

Fig-4: DFIG vector control circuit

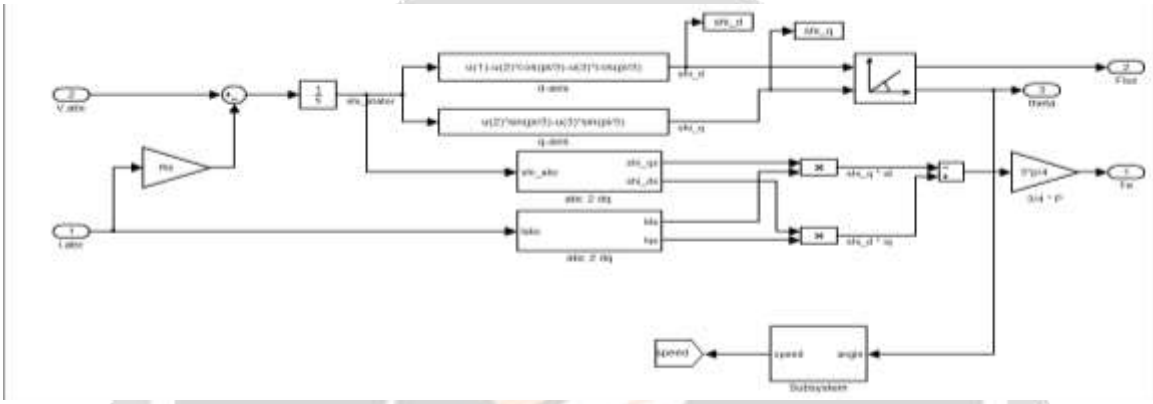

Fig-5: Torque estimation control

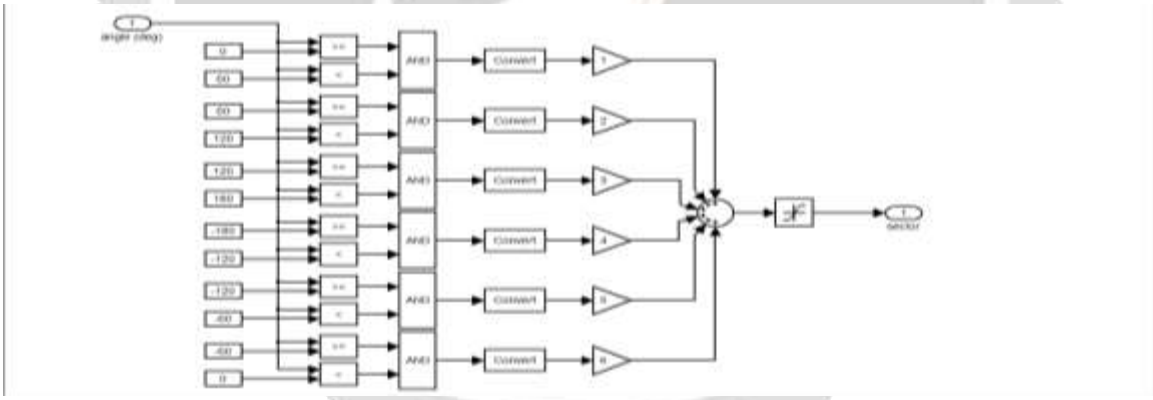

Fig-6: sector selection of the vector control

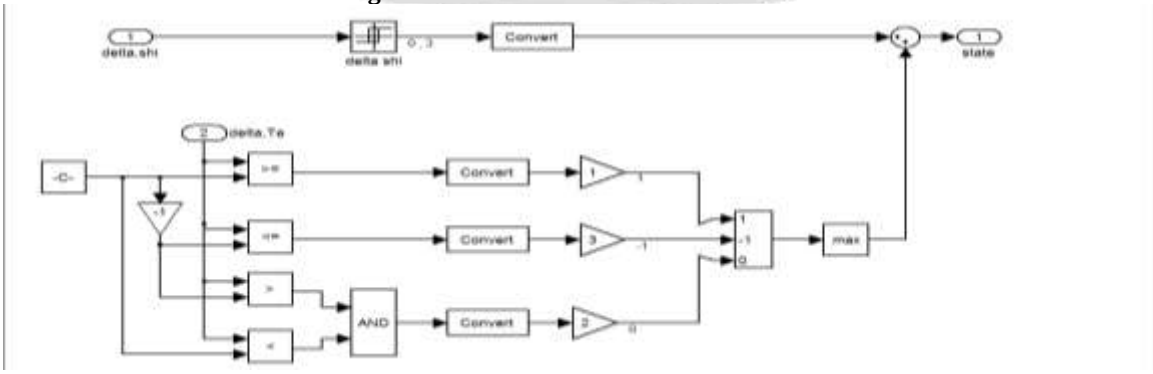

Fig-7: hysteresis control

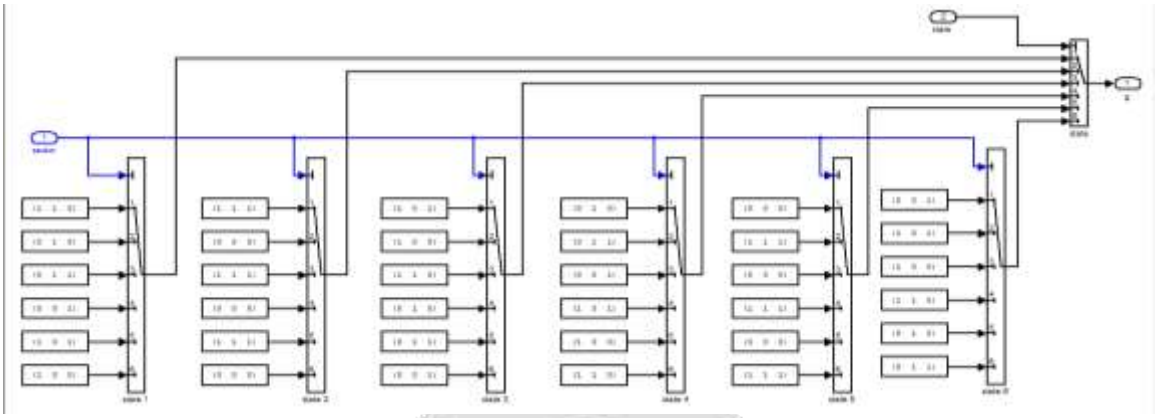

Fig-8: switch selection based on sector and state

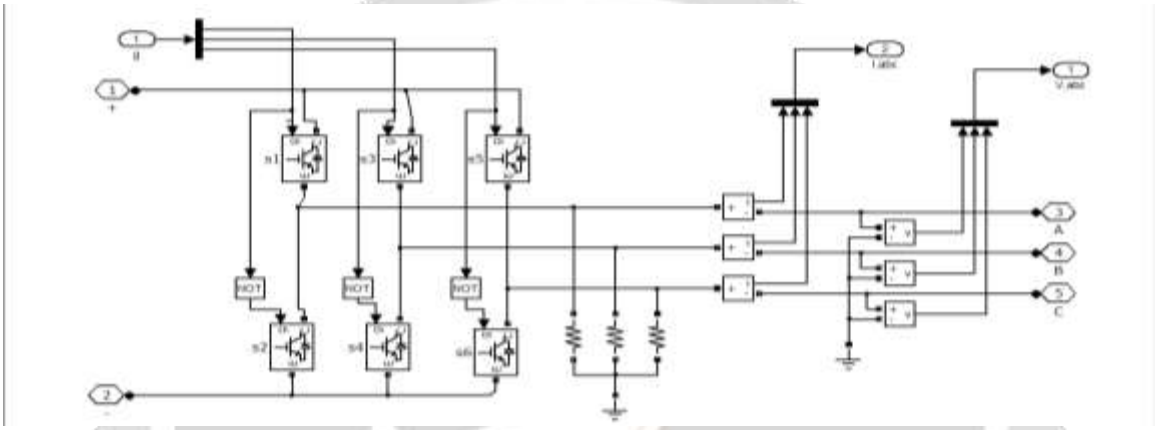

Fig-9: rotor side converter circuit

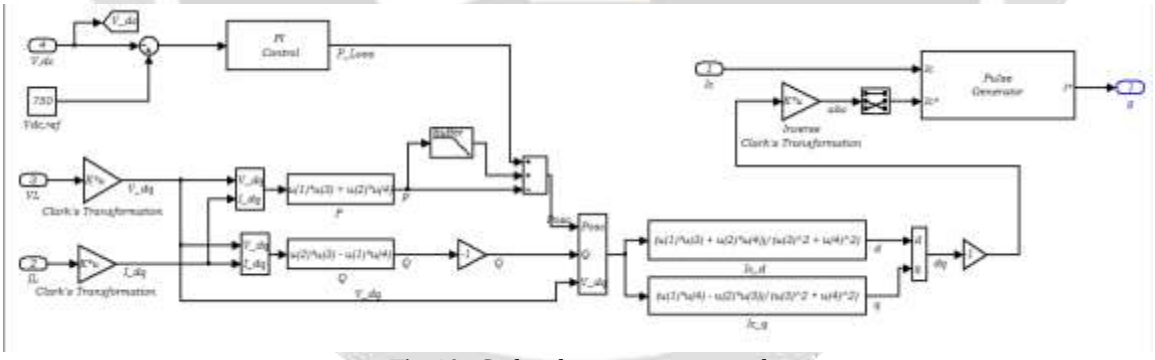

Fig-10: Grid side converter control

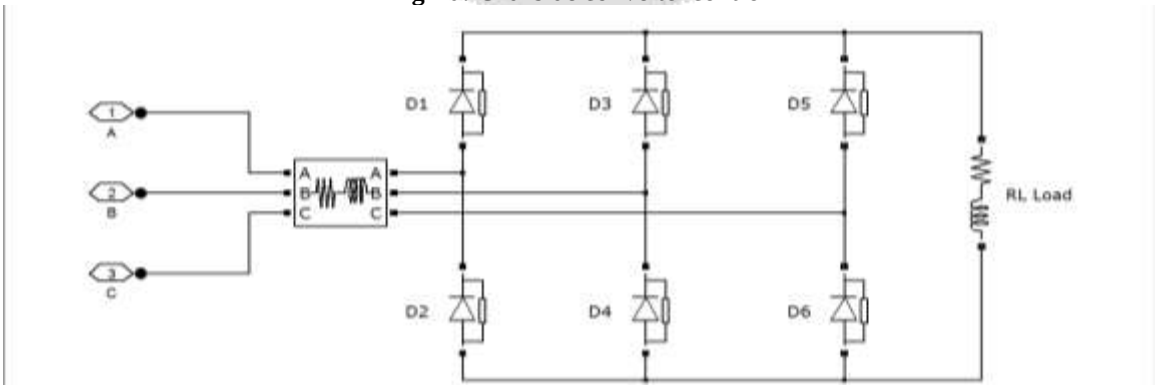

Fig-11: non-linear load

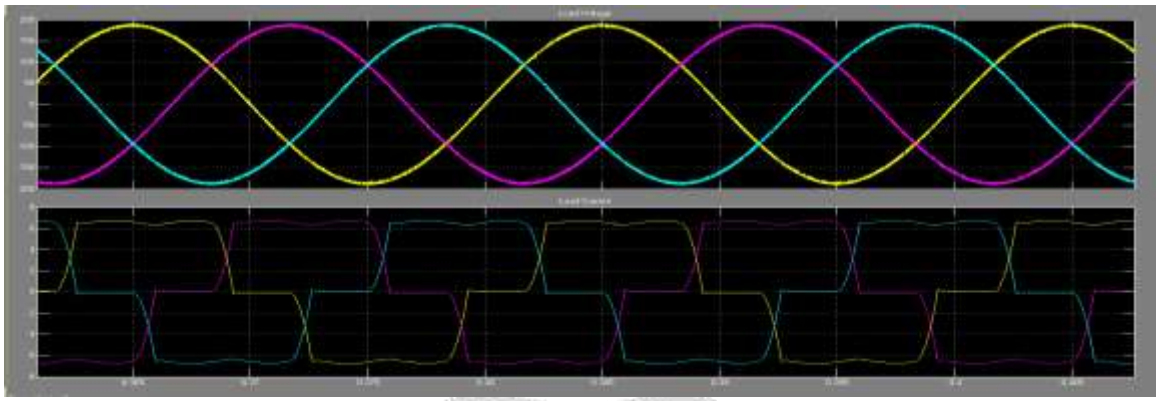

Fig-12: load voltage and load current

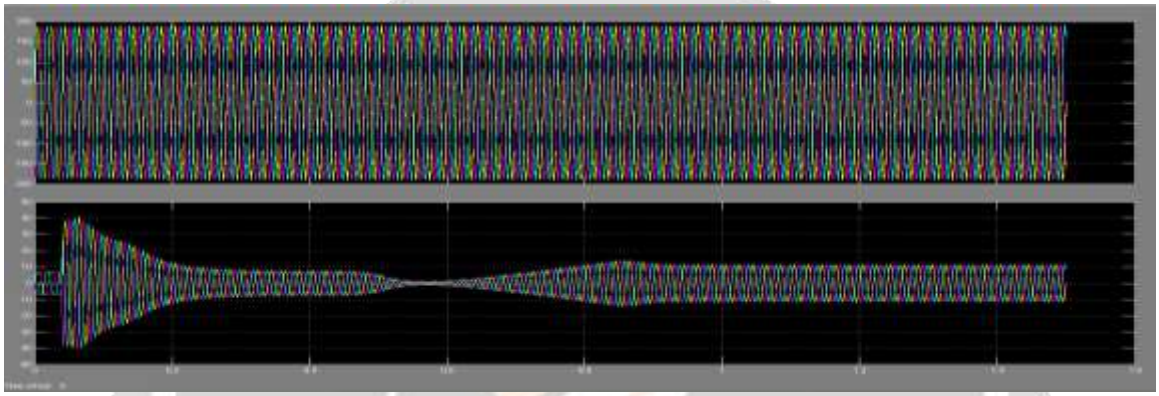

Fig-13: source voltage and source current

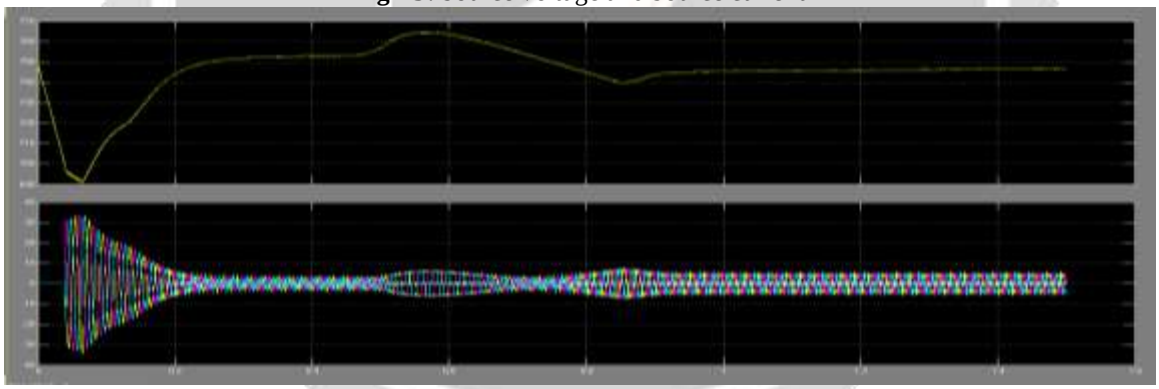

Fig-14: dc-link voltage and shunt injected current

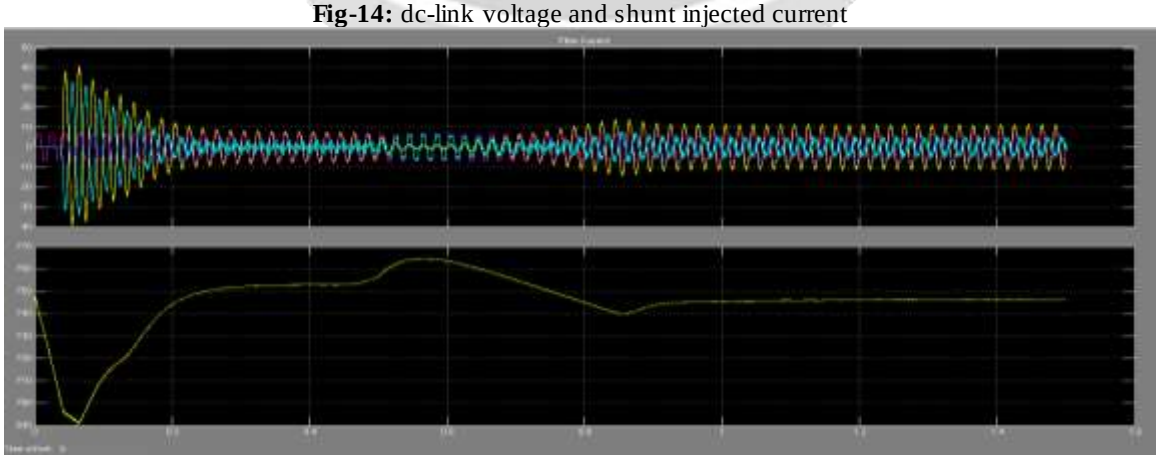

Fig-15: overall output and dc-link voltage

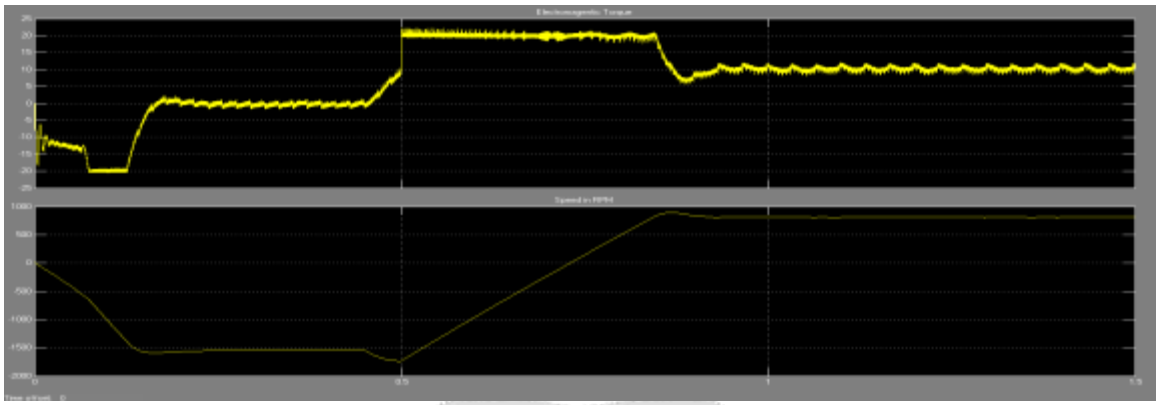

Fig-16: steady state and transient speed control verses torque

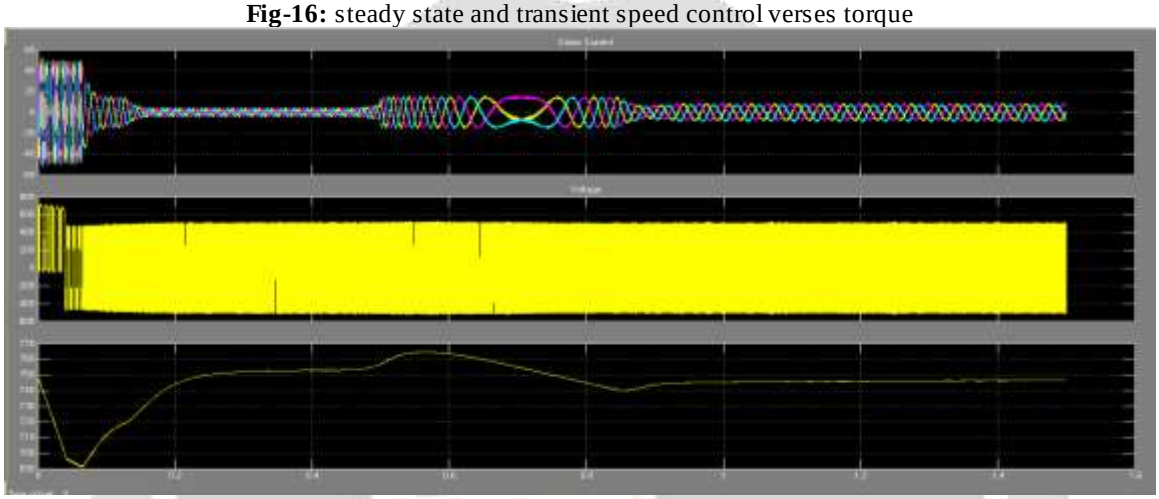

Fig-17: (i) steady state and transient speed control under zero speed, rising and falling speed conditions, (ii) inverter output voltages (iii) dc-link voltage

5. CONCLUSIONS

The GSC control algorithm of the proposed DFIG has been modified for supplying the harmonics and reactive power of the local loads. In this proposed DFIG, the reactive power for the induction machine has been supplied from the RSC and the load reactive power has been supplied from the GSC. The decoupled control of both active and reactive powers has been achieved by RSC control. The proposed DFIG has also been verified at wind turbine stalling condition for compensating harmonics and reactive power of local loads. This proposed DFIG-based WECS with an integrated active filter has been simulated using MATLAB/Simulink environment. Steady-state performance of the proposed DFIG has been demonstrated for a wind speed. Dynamic performance of this proposed GSC control algorithm has also been verified for the variation in the wind speeds and for local nonlinear load.

6. REFERENCES

[1] D. M. Tagare, *Electric Power Generation the Changing Dimensions*. Piscataway, NJ, USA: IEEE Press, 2011.

[2] G. M. Joselin Herbert, S. Iniyan, and D. Amutha, "A review of technical issues on the development of wind farms," *Renew. Sustain. Energy Rev.*, vol. 32, pp. 619–641, 2014.

[3] I.Munteanu, A. I. Bratcu, N.-A. Cutululis, and E. Ceang, *Optimal Control of Wind Energy Systems Towards a Global Approach*. Berlin, Germany: Springer-Verlag, 2008.

[4] A. A. B. Mohd Zin, H. A. Mahmoud Pesaran, A. B. Khairuddin, L. Jahanshaloo, and O. Shariati, "An overview on doubly fed induction generators controls and contributions to wind based electricity generation," *Renew. Sustain. Energy Rev.*, vol. 27, pp. 692–708, Nov. 2013.

[5] S. S. Murthy, B. Singh, P. K. Goel, and S. K. Tiwari, "A comparative study of fixed speed and variable speed wind energy conversion systems feeding the grid," in *Proc. IEEE Conf. Power Electron. Drive Syst.(PEDS'07)*, Nov. 27–30, 2007, pp. 736–743.

[6] D. S. Zinger and E. Muljadi, "Annualized wind energy improvement using variable speeds," *IEEE Trans. Ind. Appl.*, vol. 33, no. 6, pp. 1444–1447, Nov./Dec. 1997.
[7] H. Polinder, F. F. A. van der Pijl, G. J. de Vilder, and P. J. Tavner, "Comparison of direct-drive and geared generator concepts for wind turbines," *IEEE Trans. Energy Convers.*, vol. 21, no. 3, pp. 725–733, Sep. 2006.
[8] R. Datta and V. T. Ranganathan, "Variable-speed wind power generation using doubly fed wound rotor induction machine—A comparison with alternative schemes," *IEEE Trans. Energy Convers.*, vol. 17, no. 3, pp. 414–421, Sep. 2002.
[9] E. Muljadi, C. P. Butterfield, B. Parsons, and A Ellis, "Effect of variable speed wind turbine generator on stability of a weak grid," *IEEE Trans. Energy Convers.*, vol. 22, no. 1, pp. 29–36, Mar. 2007.
[10] R. Pena, J. C. Clare, and G. M. Asher, "Doubly fed induction generator using back-to-back PWM converters and its application to variable-speed wind-energy generation," *IEE Proc. Elect. Power Appl.*, vol. 143, no. 3, pp. 231–241, May 1996.
[11] S. Muller, M. Deicke, and R. W. De Doncker, "Doubly fed induction generator systems for wind turbines," *IEEE Ind. Appl. Mag.*, vol. 8, no. 3, pp. 26–33, May/Jun. 2002.
[12] W. Qiao and R. G. Harley, "Grid connection requirements and solutions for DFIG wind turbines," in *Proc. IEEE Energy 2030 Conf. (ENERGY'08)*, Nov. 17–18, 2008, pp. 1–8.
[13] A. Petersson, T. Thiringer, L. Harnefors, and T. Petru, "Modeling and experimental verification of grid interaction of a DFIG wind turbine," *IEEE Trans. Energy Convers.*, vol. 20, no. 4, pp. 878–886, Dec. 2005.
[14] H. M. Hasanien, "A set-membership affine projection algorithm-based adaptive-controlled SMES units for wind farms output power smoothing," *IEEE Trans. Sustain. Energy*, vol. 5, no. 4, pp. 1226–1233, Oct. 2014.
[15] Z. Saad-Saoud, M. L. Lisboa, J. B. Ekanayake, N. Jenkins, and G. Strbac, "Application of STATCOMs to wind farms," *IEE Proc. Gener. Transmiss. Distrib.*, vol. 145, no. 5, pp. 511–516, Sep. 1998.
[16] G. O. Suvire and P. E. Mercado, "Combined control of a distribution static synchronous compensator/flywheel energy storage system for wind energy applications," *IET Gener. Transmiss. Distrib.*, vol. 6, no. 6, pp. 483–492, Jun. 2012.